DSP-based Nonlinear Interference Estimation using Linear Least Squares Longitudinal Power Monitoring

DSP-based Nonlinear Interference Estimation using Linear Least Squares Longitudinal Power Monitoring

Lorenzo Andrenacci, Gabriella Bosco, Yanchao Jiang,
Antonino Nespola, Stefano Piciaccia and Dario Pilori

***Abstract*—A novel method for the estimation of nonlinear interference (NLI) penalties in optical networks is presented. Its theoretical derivation is grounded in linear least squares (LLS) longitudinal power monitoring (LPM), an algorithm capable of estimating the absolute power evolution of a signal along the link. We demonstrate that closed-form NLI estimation is inherently integrated into LPM. However, this method does not account for the cross-channel interference (XCI) contribution to NLI, since the receiver typically lacks knowledge of other WDM channels. To address this limitation, simple analytical expressions to compensate for the bias originating from neglecting XCI are proposed for the scenario of homogenous WDM combs. These formulas are derived from closed-form NLI models (e.g., the GN-model) and require only limited information about the signal configuration. The effectiveness of the proposed approach is validated through a wide range of realistic numerical simulations and experiments, including C-band transmissions over 300-km and 1100-km EDFA-amplified optical links. The obtained results confirm the reliability of the method, yielding nonlinear SNR estimates with a maximum absolute error consistently below 0.97 dB when compared to well-established analytical NLI models or measured values. The mean absolute errors in simulation and experiments are 0.3 dB and 0.5 dB, respectively. Additionally, a practical demonstration of transmit power optimization is provided, leveraging the values obtained through the proposed method.**

***Index Terms*—Optical Performance Monitoring, Longitudinal Power Monitoring, Nonlinear Penalty Estimation.**

I. Introduction

THE ever-increasing demand for capacity and flexibility required by modern optical communications poses an important challenge for the operation and management of today's optical networks. The capability to adapt to different traffic conditions through dynamic optical path routing and wavelength switching, the need for low-margin operation and effective network resource allocation are key challenging tasks for the designers of the communication devices. In particular, the telemetry information obtained from coherent transceivers is crucial for the monitoring and the optimization of optical networks. In fact, especially in the context of modern elastic optical networks (EONs) [1], this information can be used to automatically build and update digital twins (DTs) of the network [2], [3]. The DTs are then used to monitor, optimize and simulate the network, thanks to the availability of simple, closed-form models of the propagation of coherent signals along the fiber [4]–[6].

The digital signal processing (DSP) modules in commercial coherent transceivers already provide useful telemetry information [3]. Some of this data, such as cumulated chromatic dispersion (CD), state of polarization (SOP), and polarization-dependent loss (PDL) [7], [8], are inherently estimated by the DSP to properly perform data decoding. Additional information, like polarization-mode dispersion (PMD) and the presence of interfering WDM channels [9], can be derived through straightforward post-processing (online or offline) of the data extracted from the DSP. Moreover, this information can be obtained without the need for external monitoring instruments, e.g., optical spectrum analyzers (OSAs) and optical time-domain reflectometers (OTDRs), enabling a cost-effective and continuous stream of telemetry data from every transceiver in the network.

Among these data, the constellation signal-to-noise ratio (SNR), or – equivalently – the error vector magnitude (EVM), is one of the most important parameters. Given that the coherent optical channel can be accurately modeled as an additive white Gaussian noise (AWGN) channel [10], this parameter can precisely determine the bit error ratio (BER) or the generalized mutual information (GMI). These two metrics are directly linked to the achievable information rate (AIR) of the system after, respectively, hard-decision (HD) or soft-decision (SD) forward error correction (FEC) [11].

In an optically-amplified coherent link, there are three main noise sources: the transceiver noise, the amplified spontaneous emission (ASE) noise added by the optical amplifiers, and the nonlinear interference (NLI) noise induced by fiber Kerr nonlinearity. Segregating these noise components is crucial for the optimization of the network, as the per-span optimal optical transmit power directly depends on the ratio between NLI power and ASE power [10]. While the transceiver noise can be easily computed through a factory calibration procedure (i.e., a back-to-back measurement), isolating the ASE and NLI components presents a more complex challenge.

In the literature, several approaches have been proposed to achieve this result. Some studies exploit the fact that *a*

This work was carried out in the PhotoNext Center at Politecnico di Torino (www.photonext.polito.it) under a Sponsored Research Agreement (SRA) with Cisco Photonics Italy S.r.l.

L. Andrenacci, G. Bosco, Y. Jiang and D. Pilori are with the Dipartimento di Elettronica e Telecomunicazioni (DET), Politecnico di Torino, Corso Duca degli Abruzzi 24, 10129 Torino, Italy. e-mail: lorenzo.andrenacci@polito.it. A. Nespola is with LINKS Foundation, Via Pier Carlo Boggio 61, 10138 Torino, Italy. S. Piciaccia is with CISCO Photonics Italy S.r.l., Via Santa Maria Molgora 48/C, 20871 Vimercate (MB), Italy.

Manuscript received September 2024; Revised December 2024.

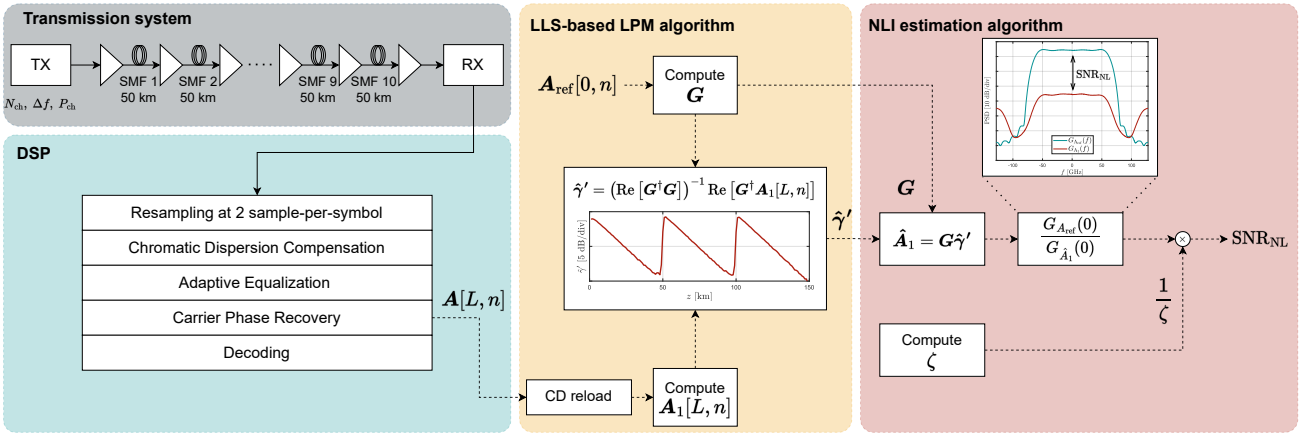

Fig. 1: Schematic of the simulation setup and DSP used to validate the proposed method. Moreover, the fundamental equations to implement LLS-based LPM and NLI estimation are also displayed.

portion of NLI does not behave as an AWGN source [12]. Under this assumption, the power of NLI can be extracted from the carrier phase recovery (CPR) algorithm [13], or from time-domain correlations in the received constellation diagram [14]–[16]. Some regression techniques are then used to obtain the actual power of NLI. However, these approaches have proved to be effective and accurate only in "ideal" situations (i.e., simulations without phase noise or experiments with strong NLI). Moreover, they require some knowledge of the link and transmission parameters to obtain the actual value of NLI.

An alternative method is presented in [17], where a calibration factor based on amplitude noise correlation is incorporated into the EVM calculation to eliminate the impact of NLI and provide an estimate of the OSNR. The main limitation of this approach is that it requires a calibration procedure before operation, and the calibration factor is dependent on both the link length and the modulation format. Another family of methods introduces notches in the time-domain [18] or in the frequency-domain [19] of the transmit signal. This category proved to be more robust and effective than the previous one. The major limitation, though, consists in the modifications and the "calibration" procedure required at the transmitter (i.e., the NLI cannot be extracted by passively monitoring the receiver DSP). The method proposed in [20], instead, leverages the spectral characteristics of ASE and NLI noises and their correlation to jointly estimate the two noise contributions. While this method still employs a calibration procedure, it does not involve modifications at the transmitter and requires in principle smaller datasets with respect to machine learning techniques (discussed in the following). However, the calibration parameters present a dependence on the potential frequency offset, the roll-off of the shaping filter and requires modifications in the case of non-central WDM channels.

Another large family of methods leverages deep learning techniques to extract the NLI directly from the received constellation [21]–[23] or SNR fluctuations due to PDL [24]. However, these approaches have several limitations. First, they are not based on physical models, making them difficult to interpret and generalize across different network scenarios. In addition, while they may offer lower computational complexity, this advantage is offset by the higher costs associated with the prior data collection step. The fundamental limitations of all these methods stem from two key factors: (1) under standard operating conditions, NLI is relatively weak, and (2) in most scenarios, the non-AWGN portion of NLI is effectively compensated by standard receiver DSP, such as CPR [25], [26]. Consequently, a different approach is needed to address this research problem.

In recent years, digital longitudinal monitoring (DLM) has emerged as a promising technique for the monitoring of optical links along the fiber propagation direction [27]–[29]. Demonstrations of DLM include the estimation of power profiles, CD maps, optical amplifier's gain spectra/tilt, optical filters' impulse response [30] and PDL [31]. Notably, DLM has proved to be a very powerful tool, requiring only the information already available in the receiver DSP and making it well-suited for integration into coherent transceivers [32]. In particular, linear least squares (LLS)-based longitudinal power monitoring (LPM) [28] is able to estimate the absolute optical power evolution of the signal along the link. This capability, when combined with simplified NLI models (e.g., the GN-model [10]), allows for accurate estimation of the NLI power. By integrating this estimate with transceiver calibration data and the overall estimated SNR, the three noise components can be effectively segregated. A first suggestion for this type of solution was made in [30], and a first implementation proposal resorts to the power profiles estimated through LPM to perform the split-step Fourier method (SSFM) and estimate NLI [33]. However, the latter involves the re-propagation of all the WDM channels, generally not available at the receiver side, which significantly increases the complexity of the method. Another possible approach consists in leveraging LPM to estimate the link parameters required for the computation of analytical NLI models (e.g., GN or EGN models). While in some cases this solution could be a viable option for the purpose of NLI estimation, it must be noted that it is an "indirect" estimation method. For this reason, potential inaccuracies in the link parameters would propagate in the NLI

model, further degrading its performance. The simple model presented in [34] could be used to quickly assess the impact of such inaccuracies on system-level metrics. In this work, extending [35], we propose an alternative and more direct approach, demonstrating how the estimation of NLI power is inherently integrated within LLS-based LPM. We then proceed to validate this approach across a wide range of simulative and experimental scenarios.

This paper is organized as follows. In Section II, we begin by briefly introducing the main concepts of the LLS LPM algorithm and then present the equations used to extract the NLI power from it. Numerical simulations in a very simplified scenario are used to show the basic features of the algorithm. Then, in Section III we present simulation results in a more realistic condition, demonstrating the potential accuracy that can be achieved in real-world scenarios. Afterward, in Section IV, we present experimental results over two different scenarios: a high-power QPSK transmission over a 300-km link and a 16-QAM transmission over 1100 km. In both cases, we demonstrate that the algorithm can achieve a good level of accuracy, suitable to be used for network optimization (e.g., computation of the optimal transmit power).

II. NLI Estimation from Linear Least Squares-based LPM

As mentioned in the Introduction, the main goal of this work is the segregation of transceiver, ASE and NLI noise contributions. We recall that, after propagation over a coherent optical link, the overall SNR (in linear units), computed on the received constellation after the DSP, can be expressed as [10]:

$$\mathrm{SNR} = (\mathrm{SNR}_{\mathrm{TRX}}^{-1} + \mathrm{OSNR}^{-1} + \mathrm{SNR}_{\mathrm{NL}}^{-1})^{-1} \tag{1}$$

where $\mathrm{SNR}_{\mathrm{TRX}}$ accounts for transceiver noise, OSNR for ASE noise and $\mathrm{SNR}_{\mathrm{NL}}$ for Kerr-induced NLI; the OSNR is computed on a reference bandwidth equal to the symbol rate. $\mathrm{SNR}_{\mathrm{NL}}$ represents the target of our estimation.

In this section, the NLI estimation method is presented. We first give a brief overview of the LLS-based LPM algorithm and show how NLI estimation is actually inherent in LPM. We proceed to derive the NLI formula and a few corrections to mitigate the estimation bias arising from such formula. A preliminary validation of all the derived expressions is also performed over a simple numerical setup.

A. Linear Least Squares-based LPM

The NLI estimation method proposed in this work relies on LLS-based LPM [28], which provides a closed-form formula of the nonlinear phase rotation (NLPR) $\gamma'(z) = \frac{8}{9}\gamma(z)P(z)$, where $\gamma(z)$ is the fiber nonlinear coefficient and $P(z)$ is the signal power at position z. Assuming that $\gamma(z)$ is known, the signal power profile can be simply computed from NLPR as $P(z) = \frac{9}{8}\frac{\gamma'(z)}{\gamma(z)}$.

The estimation of $\gamma'(z)$ can be formulated as a nonlinear least squares optimization problem [30], given the received signal $\boldsymbol{A}[L,n]$ and a reconstructed version of the transmitted (or reference) signal $\boldsymbol{A}_{\mathrm{ref}}[0,n]$ as boundary conditions:

$$\hat{\boldsymbol{\gamma}}' = \underset{\boldsymbol{\gamma}'}{\operatorname{argmin}} \|\boldsymbol{A}[L,n] - \boldsymbol{A}_{\mathrm{ref}}[L,n]\|^2. \tag{2}$$

In (2), $\boldsymbol{A}_{\mathrm{ref}}[L,n]$ is the virtually-propagated reference signal, L is the link length and $n = t/T_s$ is the discrete-time index with respect to the sampling period T_s. In this case, $\boldsymbol{\gamma}' = \left[\gamma'_0, \ldots, \gamma'_k, \ldots, \gamma'_{K-1}\right]^T$ with $\gamma'_k = \gamma'(z_k)$ ($k \in [0, K-1]$, $z_0 = 0$ and $z_{K-1} = L$). This problem can be made linear resorting to the first-order enhanced regular perturbation (eRP1) [36], [37] approximation. According to eRP1, both received and virtually-propagated reference signals can be expressed as:

$$\begin{aligned} \boldsymbol{A}[L,n] &\simeq \boldsymbol{A}_0[L,n] + \boldsymbol{A}_1[L,n] \\ \boldsymbol{A}_{\mathrm{ref}}[L,n] &\simeq \boldsymbol{A}_{\mathrm{ref},0}[L,n] + \boldsymbol{A}_{\mathrm{ref},1}[L,n]. \end{aligned} \tag{3}$$

The two terms $\boldsymbol{A}_0[L,n]$ and $\boldsymbol{A}_1[L,n]$ in (3) represent the linear term after applying the total cumulated CD and the first-order approximation of the Kerr effect, respectively. Specifically, the two terms of the approximation for $\mathbf{A}_{\mathrm{ref}}[L,n]$ are computed as

$$\begin{aligned} \boldsymbol{A}_{\mathrm{ref},0}[L,n] &= \mathrm{D}_{0,L}\left[\boldsymbol{A}_{\mathrm{ref}}[0,n]\right] \\ \boldsymbol{A}_{\mathrm{ref},1}[L,n] &= \boldsymbol{G}\boldsymbol{\gamma}' \end{aligned} \tag{4}$$

where each column $\boldsymbol{g}_k$ of the perturbation matrix $\boldsymbol{G} = [\boldsymbol{g}_0, \ldots, \boldsymbol{g}_k, \ldots, \boldsymbol{g}_{K-1}]$ is defined as

$$\boldsymbol{g}_k = -j\Delta z_k \cdot \mathrm{D}_{z_k,L}\left[\mathrm{N}_p\left[\mathrm{D}_{0,z_k}\left[\boldsymbol{A}_{\mathrm{ref}}[0,n]\right]\right]\right]. \tag{5}$$

In (5), $\mathrm{D}_{z_i,z_j}[\cdot]$ is a linear operator which introduces CD from position z_i to z_j, $\mathrm{N}_p[\cdot] = \left(\|\cdot\|^2 - \frac{3}{2}P_A\right)(\cdot)$ is a nonlinear operator, with P_A being the average power of $\boldsymbol{A}_{\mathrm{ref}}[z,n]$, and $\Delta z_k = z_{k+1} - z_k$ is the spatial step. Note that $\boldsymbol{A}_0[L,n] \simeq \boldsymbol{A}_{\mathrm{ref},0}[L,n]$, if the sampling rate satisfies the Nyquist criterion. This makes the derivation of $\boldsymbol{A}_1[L,n]$ in (3) straightforward. We would like to highlight the fact that the Nyquist criterion is required to accurately re-construct $\boldsymbol{A}_{\mathrm{ref},0}[L,n]$. However, relaxations to this assumption have been proposed and demonstrated [32], [38], in which LPM is performed leveraging symbol-rate data. While this solution reduces the complexity of the algorithm, it comes at the cost of a calibration procedure that needs to be performed before operation [38]. For the purpose of this work, the Nyquist criterion will be considered valid in all cases. Substituting (3) and (4) in (2), the nonlinear optimization problem reduces to an LLS optimization problem:

$$\hat{\boldsymbol{\gamma}}' = \underset{\boldsymbol{\gamma}'}{\operatorname{argmin}} \left\|\boldsymbol{A}_1[L,n] - \boldsymbol{G}\boldsymbol{\gamma}'\right\|^2. \tag{6}$$

whose closed-form solution is yielded by

$$\hat{\boldsymbol{\gamma}}' = \left(\mathrm{Re}\left[\boldsymbol{G}^\dagger\boldsymbol{G}\right]\right)^{-1}\mathrm{Re}\left[\boldsymbol{G}^\dagger\boldsymbol{A}_1[L,n]\right]. \tag{7}$$

$\mathrm{Re}(\cdot)$ and $(\cdot)^\dagger$ represent the real part and Hermitian transpose operators, respectively. Equations (6) and (7) are fundamental for the following derivation of the NLI estimation formulas.

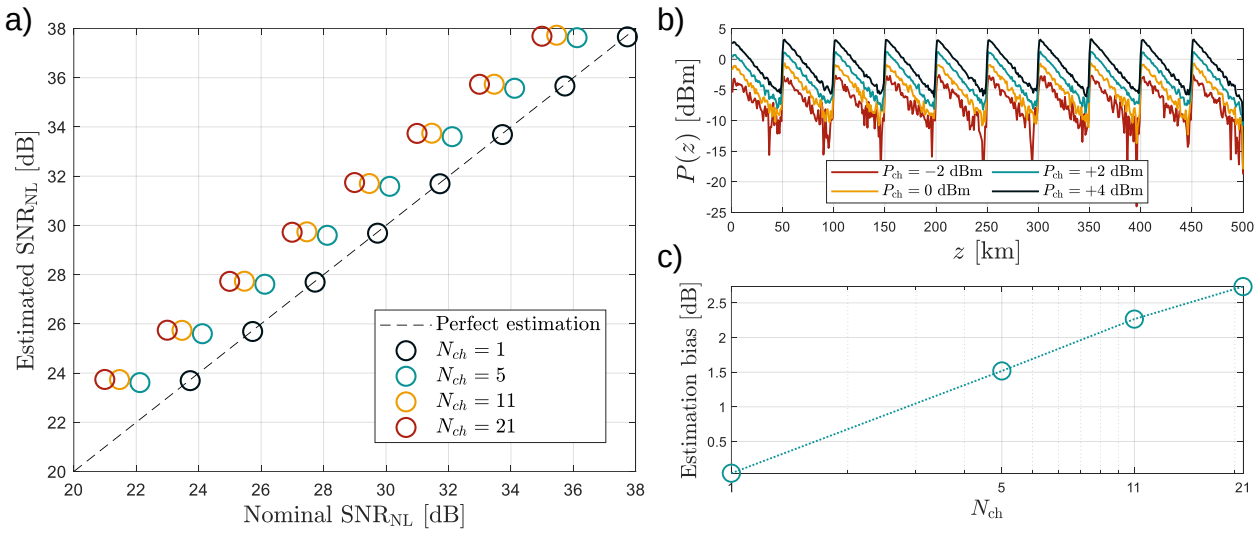

Fig. 2: a) Results of $\mathrm{SNR}_{\mathrm{NL}}$ estimation using (10) (circles) and the GN-model (black dashed line) over a 10×50-km SMF link at 128 GBaud per channel and $\Delta f = 200\,\mathrm{GHz}$ for a varying number of WDM channels N_{ch}. b) Example of estimated power profiles in the single channel scenario. c) Mean estimation bias with respect to nominal $\mathrm{SNR}_{\mathrm{NL}}$ computed with GN-model.

B. NLI Estimation Algorithm

The overall information on NLI is carried by the term $\boldsymbol{A}_1[L,n]$ in (3). According to eRP1, the received cumulated NLI is simply the sum of all the local NLI contributions $\boldsymbol{g}(z)\gamma'(z)$ at position z in the link, after applying the remaining CD (see (5)), and can be expressed as

$$\boldsymbol{A}_1(L,t) = \int_0^L \boldsymbol{g}(z,t)\gamma'(z)\,\mathrm{d}z. \tag{8}$$

where t is the continuous time instant. Note that the expression in (4) is simply the discretized version of (8), where $\boldsymbol{g}_k = \boldsymbol{g}(z_k,n)$, $\gamma'_k = \gamma'(z_k)$ and $\Delta z_k = \mathrm{d}z$.

The idea at the basis of the proposed NLI estimation method is to get an estimate of this perturbation term and use it to retrieve the corresponding $\mathrm{SNR}_{\mathrm{NL}}$. To this purpose, it is possible to notice that such estimation is actually intrinsic to the LLS-based LPM algorithm. The LLS optimization problem in (6) aims to find the $\boldsymbol{\gamma'}$ that minimizes the difference between $\boldsymbol{A}_1[L,n]$ and $\boldsymbol{A}_{\mathrm{ref},1}[L,n]$ in the least-square sense. Hence, computing $\hat{\boldsymbol{\gamma}}'$ from (7) and multiplying it by $\boldsymbol{G}$ results in an estimate – in discrete time – of (8):

$$\hat{\boldsymbol{A}}_1[L,n] = \boldsymbol{G}\hat{\boldsymbol{\gamma}}' \tag{9}$$

It is then straightforward to compute $\mathrm{SNR}_{\mathrm{NL}}$. Let us define the power spectral densities (PSDs) of (9) and the reference signal as $G_{\hat{A}_1}(f)$ and $G_{A_{\mathrm{ref}}}(f)$, respectively. Under the assumption that the PSD is flat over the band of interest, $\mathrm{SNR}_{\mathrm{NL}}$ can be computed as:

$$\mathrm{SNR}_{\mathrm{NL}} = \frac{G_{A_{\mathrm{ref}}}(0)}{G_{\hat{A}_1}(0)} \tag{10}$$

Both (9) and (10) provide several advantages. In the first place, they are closed-form formulas. This eliminates the need for SSFM (or other numerical techniques) to estimate the nonlinear noise. Moreover, the impact of ASE noise is limited since it only affects $\hat{\boldsymbol{\gamma}}'$ in (9) and can be mitigated resorting to successive profile averaging and/or increasing the number of samples employed in the LPM algorithm [28]. Lastly, the required knowledge of the system is – in principle – restricted only to the cumulated CD, which is generally available in coherent transceivers at the CDC stage or can be easily estimated [39].

C. Preliminary Validation

A preliminary numerical validation is performed over the simple setup in Fig. 1, in which all the fundamental steps to implement LLS-based LPM and NLI estimation are also displayed. It consists of a WDM comb of dual polarization (DP) 64-QAM channels, modulated at a symbol rate $R_s = 128$ Gbaud, and shaped by a square-root raised-cosine (SRRC) filter (roll-off $\rho = 0.1$). The simulations are carried out considering the main parameters spanning in the following ranges: number of channels $N_{\mathrm{ch}} \in \{1,\ 5,\ 11,\ 21\}$, per-channel power $P_{\mathrm{ch}} \in \{-2, \ldots, +5\}$ dBm and channel spacing $\Delta f \in \{150,\ 175,\ 200\}$ GHz. The channel of interest (COI) is the center channel, if not specified otherwise. The link is composed of 10×50-km identical spans of G.652 single mode fibers (SMFs), with attenuation $\alpha_{\mathrm{dB}} = 0.2\,\mathrm{dB/km}$, CD coefficient $\beta_2 = -21.28\,\mathrm{ps}^2/\mathrm{km}$ and nonlinearity coefficient $\gamma = 1.3\ 1/\mathrm{W/km}$. Each span is followed by an EDFA with noise figure $F = 5\,\mathrm{dB}$ to fully compensate for the span loss. Fiber propagation is modeled according to our internal SSFM implementation [40]. The received signal is then processed by a standard DSP chain, which includes resampling at 2 sample-per-symbol, CD compensation (CDC), adaptive equalization and CPR. The output of the CPR stage is finally extracted and used as input for the LLS-based LPM and the subsequent NLI estimation algorithm. All results are compared to those obtained with a GN-model [41] running in parallel to the numerical simulations and used as a reference. Note that the

implemented version of the GN model does not take into account the impact of the modulation format.

All combinations of values for N_{ch} and P_{ch} were tested, while keeping the channel spacing constant at $\Delta f = 200\,\mathrm{GHz}$. The results are reported in Fig. 2(a), while an example of the power profiles utilized in the NLI estimation algorithm is shown in Fig.2(b), for $N_{\mathrm{ch}} = 1$. The estimation is very accurate for the single-channel case; however an estimation bias appears when the number of WDM channels increases, as displayed in Fig. 2(c). In fact, the major limitation of the proposed method derives from the LPM algorithm itself, since LPM only leverages self-channel interference (SCI) [41] for power profile estimation. All other sources of stochastic noise, such as ASE or laser phase noise, or static distortions from transceiver implementation, are seen as noise by the LPM algorithm. Among these sources of noise, cross-channel interference (XCI) is also included. In general, no knowledge of the interfering WDM channels is available at the receiver side and only the COI is virtually-propagated in the LPM algorithm. Hence, it is not possible to estimate the XCI contribution to the total NLI. Although multichannel LPM has recently been proposed [42], [43] to include both the SCI and XCI contributions in the power profile estimation, it comes at the cost of an increased complexity and may not be feasible when the number of WDM channels is large, e.g., full C-band transmissions. For this reason, we will present a few examples of solutions to this problem in the form of a simple correction factor applied to (10), based on the knowledge of some system parameters.

D. Estimation Bias Correction

It has been demonstrated in Sec. II-C that the LLS-based algorithm only estimates the NLI power generated by the nonlinear beating of the COI with itself i.e., the SCI. However, there are two other sources of the NLI that need to be accounted for, namely XCI and multichannel interference (MCI). In the context of long-distance high-symbol-rate (i.e., ≥ 60 GBaud) multi-channel transmission over uncompensated SMF links, MCI is negligible [44]–[46]; however, XCI cannot be neglected. Therefore, in order to obtain the power of the overall NLI, the XCI power must be evaluated.

Without any loss of generality, we can define an "XCI correction factor" ζ as:

$$P_{\mathrm{NLI}} \approx P_{\mathrm{SCI}} + P_{\mathrm{XCI}} = P_{\mathrm{SCI}} \left(1 + \frac{P_{\mathrm{XCI}}}{P_{\mathrm{SCI}}}\right) = P_{\mathrm{SCI}} \cdot \zeta \quad (11)$$

With the knowledge of ζ and P_{SCI}, the full NLI power P_{NLI} can be estimated, obtaining a full segregation of the noise source. Moreover, including ζ into (10), the expression for $\mathrm{SNR}_{\mathrm{NL}}$ becomes:

$$\mathrm{SNR}_{\mathrm{NL}} = \frac{1}{\zeta} \frac{G_{A_{\mathrm{ref}}}(0)}{G_{\hat{A}_1}(0)}. \quad (12)$$

If all the parameters of the link are known, ζ can be easily obtained by using any NLI model. For instance, if we consider as COI the central channel of a homogeneous WDM comb, comprising N_{ch} channels with a symbol rate R_{s} and spaced by Δf, we can apply the straightforward closed-form approximation provided by the GN model [41, Eq. (15)], yielding

$$\zeta \approx \frac{\operatorname{asinh}\left(\frac{\pi^2}{2}\beta_2 L_{\mathrm{eff,a}} R_{\mathrm{s}}^2 N_{\mathrm{ch}}^{\frac{2R_{\mathrm{s}}}{\Delta f}}\right)}{\operatorname{asinh}\left(\frac{\pi^2}{2}\beta_2 L_{\mathrm{eff,a}} R_{\mathrm{s}}^2\right)}. \quad (13)$$

This expression depends on the symbol rate and the frequency spacing of the channel, as well as on the fiber's dispersion (β_2) and attenuation ($L_{\mathrm{eff,a}} = 1/2\alpha$, where α is the field attenuation parameter). Then, assuming "standard" conditions

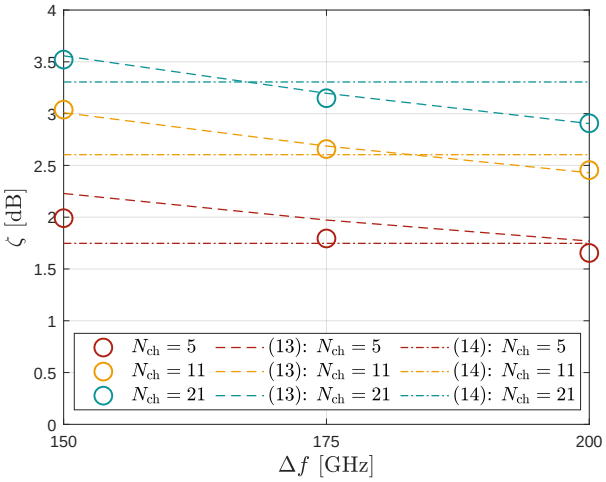

Fig. 3: Accuracy of ζ from (13) (dashed line) and (14) (dash-dotted line) for varying number of channels N_{ch} and channel spacing Δf compared to previously computed estimation bias arising from (10) (circles).

(i.e., transmission over SMF of modern coherent optical channels), in [34, Eq. (23)] the authors provided an even simpler approximation, which was also adopted in [35]:

$$\zeta \approx \sqrt[4]{N_{\mathrm{ch}}}. \quad (14)$$

The introduced error is relatively large due to the higher level of approximation. However, it proves effective while requiring only the knowledge of a single additional transmission parameter. A comparison between the two approaches is displayed in Fig. 3, where the mean estimation bias arising from (10) is reported for several combinations of N_{ch} and Δf.

We stress the fact that both (13) and (14) have been derived under the assumption of homogeneous WDM combs. This is the assumption that has been made in II-C, as well as in all the following sections. It is a reasonable assumption for terrestrial WDM applications leveraging ASE noise loading [47] and ROADMs to equalize the relative power of the WDM channels along the network, for instance. In the case of specific applications that require a different power loading strategy and/or coarsely-spaced WDM channels, more comprehensive NLI models are to be employed to also account for these aspects. Nevertheless, it is important to remark that all these approximations do not require the knowledge of the nonlinear parameter γ, which is generally hard to estimate. Both approximations, though, assume that the COI is the

central WDM channel. Potentially, an expression of ζ for other channels may be obtained from closed-form equations of NLI models. However, such expression would be quite long, albeit in closed-form. As it will be shown in the next section, for the specific purpose of noise segregation in the context of modern, high symbol rate ($\geq$ 60 GBaud), coherent transmission, an accurate estimation of ζ is actually not required. Therefore, we try to obtain a rough approximation of ζ, by adding a correction term to (14), yielding

$$\log_{10}(\zeta) \approx \frac{1}{4}\log_{10}(N_{\mathrm{ch}}) + a\left[\log_{10}\left(\frac{B_{\mathrm{L}}}{B_{\mathrm{R}}}\right)\right]^2. \qquad (15)$$

In this equation, B_{L} and B_{R} are, respectively, the optical bandwidth at the left and right of the COI. The parameter a can be estimated through a simple linear regression from a dataset of results, similar to the procedure followed in [34]. To do this, we built a dataset comprising 1 440 different scenarios, by changing the number of 64-GBaud WDM channels from 3 to 45, and the number of SMF spans from 1 to 20. For each span in each scenario, the length L_s, attenuation and dispersion were randomly selected, assuming a Gaussian distribution with a standard deviation of 5% relative to the nominal values of $L_s = 70\,\mathrm{km}$, $\alpha_{\mathrm{dB}} = 0.2\,\mathrm{dB/km}$ and $\beta_2 = -22.77\,\mathrm{ps}^2/\mathrm{km}$.

All scenarios were simulated using the CFM NLI model [5], and the value ζ was extracted for each of them. After applying a linear regression on (15), we obtained $a \approx -0.0475$. We remark that, although this is a quite rough approximation of ζ, it is a simple linear expression that requires the minimum amount possible of parameters. Moreover, its applicability remains limited to C-band transmissions, since in UWB scenarios, such as C+L transmissions, the impact of inter-channel stimulated Raman scattering (ISRS) cannot be neglected. Its effectiveness will be discussed in Sec. III considering more realistic simulation scenarios. As mentioned above, when a more accurate estimation of ζ is required, standard NLI models (assuming that the parameters are known or can be estimated) can be used.

III. Numerical Simulations

In this section, we provide a thorough numerical validation of the proposed method across two different system configurations. Specifically, we account for non-central WDM channels, implement a more realistic fiber propagation model, and consider a transmission distance that aligns more closely with the typical reach of the employed modulation format.

A. Simulation Setup

The first configuration for the transmitted DP-16QAM WDM signal consists of $N_{\mathrm{ch}} = 30$ channels at $R_s = 64$ Gbaud spaced by $\Delta f = 100\,\mathrm{GHz}$, while the second one of $N_{\mathrm{ch}} = 15$ channels at $R_s = 128$ Gbaud spaced by $\Delta f = 200\,\mathrm{GHz}$. The pulses are shaped with an SRRC filter with roll-off $\rho = 0.1$. To test different values of $\mathrm{SNR}_{\mathrm{NL}}$, the per-channel power has been varied between $-1\,\mathrm{dBm}$ and $5\,\mathrm{dBm}$ with a $2\,\mathrm{dB}$ step. Note that this range includes the optimal power for both configurations.

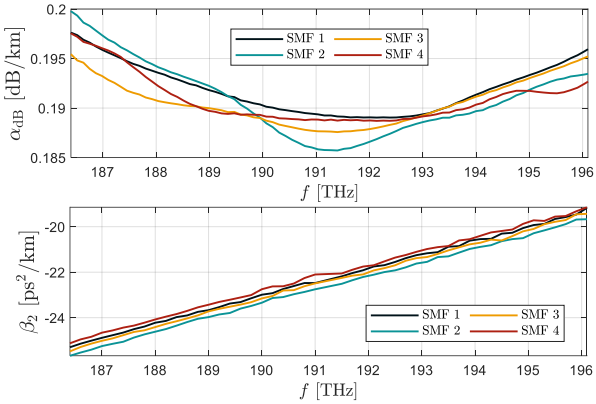

Fig. 4: Measurements of frequency-dependent power attenuation coefficient α_{dB} and chromatic dispersion coefficient β_2 of the four SMF fibers used in the simulation setup.

Moreover, a laser phase noise characterized by a linewidth of $\Delta\nu = 50\,\mathrm{kHz}$ is introduced and modeled as a Wiener process. The signal is then propagated over a 17×65-km SMF optical link, where each span is terminated by an EDFA with noise figure $F = 5\,\mathrm{dB}$ that fully recovers the span loss and equalizes the per-channel power. We consider frequency-dependent power attenuation α_{dB} and dispersion β_2, with values derived from four experimentally characterized G.652 SMF fiber spans, as shown in Fig. 4. In the numerical setup, these four fiber spans are repeatedly alternated, thus emulating a recirculating loop. ISRS is also considered, even though its effect is almost negligible, given the relatively small optical bandwidth (i.e., 3 THz). The received signal is resampled at a rate of 2 samples-per-symbol and processed by a standard DSP. This includes CDC, least-mean-square (LMS)-based adaptive equalization and blind phase search (BPS) CPR. The output of this last stage is extracted and used as input for LPM and the subsequent NLI estimation algorithm. Approximately 2^{17} samples are used for LPM with spatial steps set to $\Delta z = 2\,\mathrm{km}$ and $\Delta z = 1\,\mathrm{km}$ for the two configurations. $\mathrm{SNR}_{\mathrm{NL}}$ is estimated leveraging (12) and (15) from a subset of 7 and 6 channels, respectively. Since all the parameters are known, a GN-model [41] is run to compare the estimated $\mathrm{SNR}_{\mathrm{NL}}$ values with those obtained with an accurate NLI model.

B. Results and Discussion

The results for the 64-Gbaud and 128-Gbaud configurations are presented in Fig. 5(a) and Fig. 5(b), respectively. In both cases, the estimated $\mathrm{SNR}_{\mathrm{NL}}$ values are consistent with those obtained with the GN-model, used as a reference. Some oscillations are present, probably due to the more challenging environment in which the LPM algorithm is applied. The power profiles used to compute (9) are extremely noisy due to the large amount of ASE noise that is cumulated during propagation. In addition, other impairments contribute to the degradation of such profiles, such as the presence of phase noise. However, the deteriorated performance of LPM does not seem to degrade too much the accuracy of the proposed method. In fact, the mean absolute error with respect to the

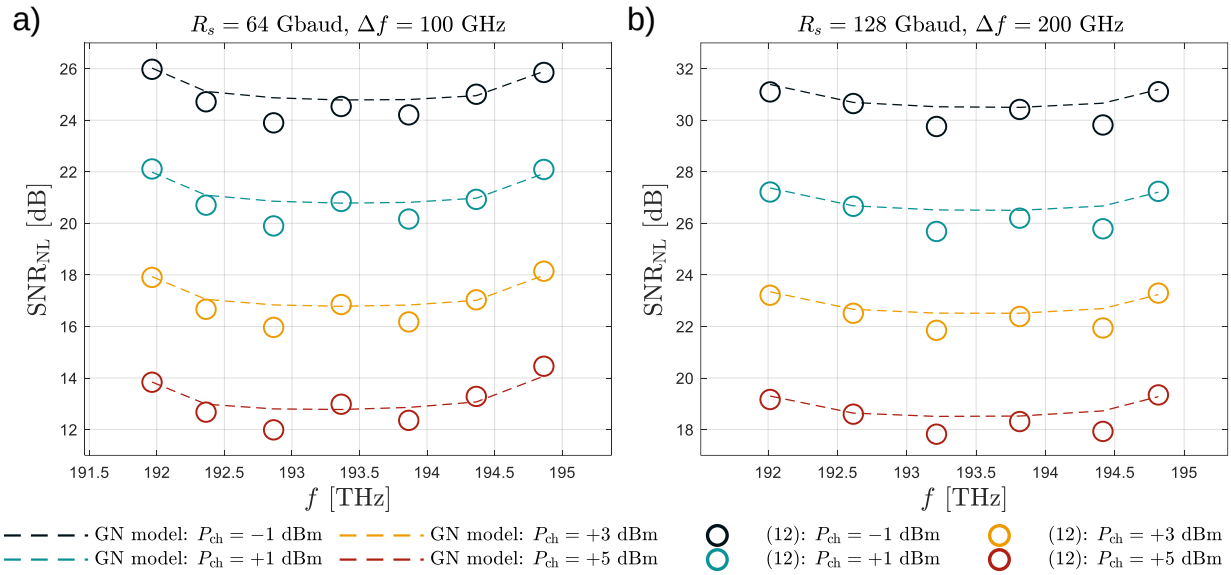

Fig. 5: Numerical results of $\mathrm{SNR}_{\mathrm{NL}}$ estimation with (12) over a 17×65-km SMF link under two system configurations: a) $N_{\mathrm{ch}} = 30$, $R_s = 64$ Gbaud and $\Delta f = 100\,\mathrm{GHz}$; b) $N_{\mathrm{ch}} = 15$, $R_s = 128$ Gbaud and $\Delta f = 200\,\mathrm{GHz}$. In both configurations, $P_{\mathrm{ch}} \in \{-1,\ +1,\ +3,\ +5\}$ dBm.

reference curves is around $0.3\,\mathrm{dB}$ in both conditions, whereas the maximum absolute errors are $0.97\,\mathrm{dB}$ and $0.88\,\mathrm{dB}$, respectively. Moreover, the estimated values manage to follow the correct evolution of NLI across all the tested conditions and for all COIs. This is also a validation of (15) which proves effective in correcting the different XCI contributions for the non-central channels, which generally experience a weaker XCI impact due to the lower number of neighboring channels. A further validation is provided in Section IV-B where a setup with the same characteristics is used to test the proposed method in an experimental scenario.

To conclude, we emphasize that the required accuracy of the XCI correction term becomes less critical as the symbol rate increases. In this section, the results presented were obtained with symbol rates of 64 and 128 GBaud, corresponding to 30 and 15 WDM channels, respectively. For the central channels, which are the most affected by XCI, the values of ζ are $3.7\,\mathrm{dB}$ and $2.9\,\mathrm{dB}$ for these two cases. This indicates that the relative intensity of XCI in comparison to SCI decreases as the symbol rate increases (or equivalently, as the number of channels decreases) [48]. Considering the current industrial trend to increase the symbol rate (e.g., see [49] for the case of 200-GBaud transceivers), the ratio of XCI to SCI, represented by ζ, is expected to further decrease. These considerations are based on the analyzed simulation scenario, in which the total WDM bandwidth is approximately $\sim 3\,\mathrm{THz}$, but can be extended to full C-band transmissions using (15).

IV. Experimental Validation

After validating the algorithm with numerical simulations, we test its accuracy over two different experimental scenarios. The first experiment was conducted over a link designed to work in a condition where LPM algorithms – in general – work well [29] (i.e., short distance, high transmit power and small optical bandwidth). In the second experiment, we explored a more realistic scenario, where the transmission distance approaches the maximum reach of the employed modulation format.

In both scenarios, the experiments were performed using commercial coherent transceivers over two different straight transmission lines. Although the proposed algorithm was implemented off-line, its predictions are compared with the SNR provided by the receiver's real-time DSP, offering a realistic estimate of the actual SNR achievable in deployed networks.

A. Transmission over a 300-km Link

The setup displayed in Fig. 6(a) is used to experimentally validate the proposed method. The COI is a DP-QPSK 64-Gbaud signal, shaped by an SRRC filter with roll-off 0.1 and centered at $f = 193.3\,\mathrm{THz}$. A WaveShaper (WS) is placed after an ASE source to generate the interfering WDM channels [50], producing a WDM comb with 18 channels spaced by $100\,\mathrm{GHz}$ across the C band. The signal is amplified with a first EDFA acting as booster (BST) and propagated through an optical link consisting of $N = 5$ standard single-mode fiber (SSMF) spans with a nominal length of $L_s = 60\,\mathrm{km}$. An in-line EDFA (ILA), working in automatic gain control mode and compensating for the previous span loss, terminates each span. To monitor the PSD evolution of the propagating WDM signal, the monitoring ports of the EDFAs and the $90/10$ splitters placed at the end of each span are connected to an OSA. At the receiver side, the COI is filtered by a tunable optical filter (TOF) centered at the COI center frequency and attenuated by a VOA to adjust its power before entering the commercial transceiver. It is then sampled at 96 GSa/s by the transceiver's analog-to-digital converter (ADC) and the acquired samples are downloaded for offline processing. After

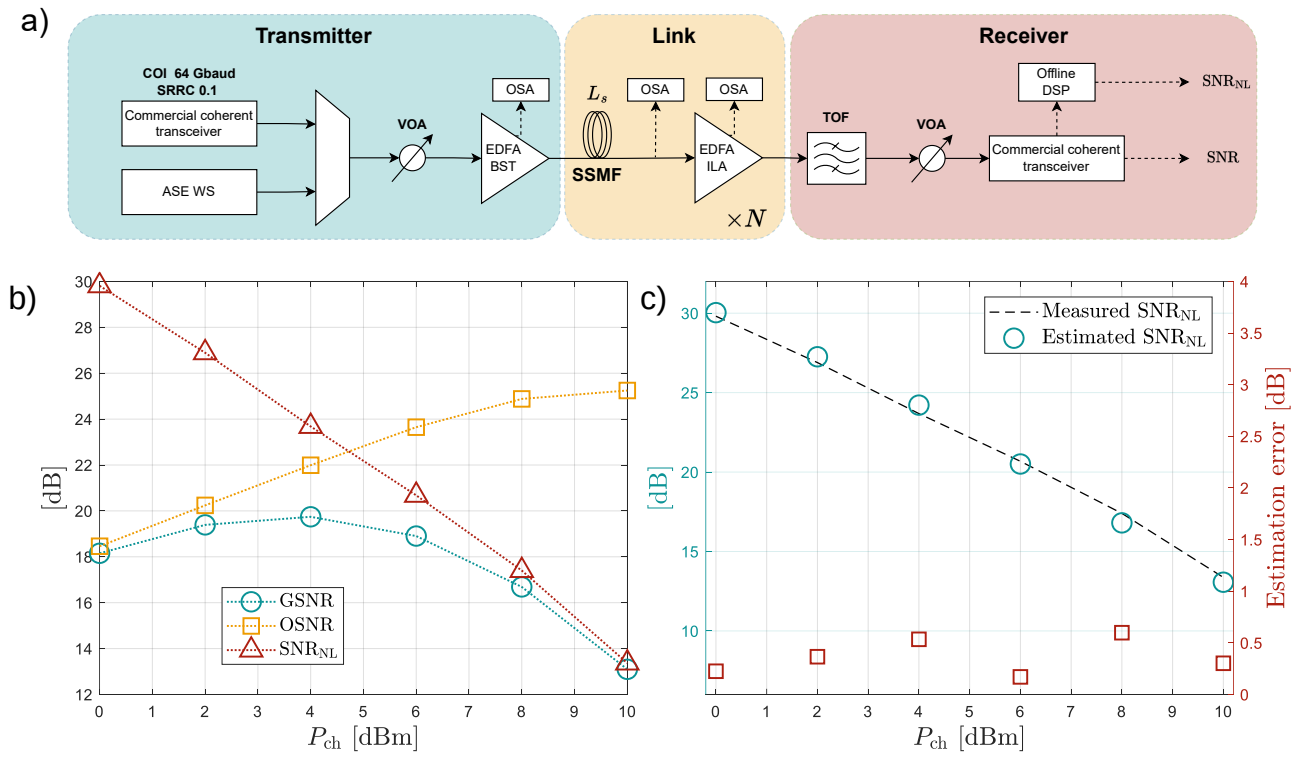

Fig. 6: a) Experimental setup. WS: wave shaper; VOA: variable optical attenuator; BST: booster; OSA: optical spectrum analyzer; ILA: in-line amplifier; TOF: tunable optical filter. b) Measured GSNR, OSNR and $\mathrm{SNR}_{\mathrm{NL}}$ for each tested per-channel power P_{ch}. c) Comparison between measured (dashed black) and estimated (blue circles) $\mathrm{SNR}_{\mathrm{NL}}$ with corresponding absolute estimation error (green squares).

front-end corrections and resampling at a rate of 2 sample-per-symbol, the signal samples enter the coherent DSP, where CDC, frequency offset compensation (FOC), LMS-based 2×2 MIMO fractionally-spaced equalization and Viterbi-Viterbi (4-th power) CPR are performed. The output of the CPR stage is then extracted, CD is reloaded and the signal is fed to the LPM algorithm. The number of samples used as input is 2^{17} and the spatial resolution is set to $\Delta z = 2\,\mathrm{km}$.

In order to span over a wide range of $\mathrm{SNR}_{\mathrm{NL}}$ values, the per-channel power P_{ch} has been varied between $0\,\mathrm{dBm}$ and $+10\,\mathrm{dBm}$, with a step of $2\,\mathrm{dB}$, by using a variable optical attenuator (VOA) placed before the BST EDFA. For each tested condition, 100 profiles have been estimated and used in the computation of (9) and (12) for the estimation of $\mathrm{SNR}_{\mathrm{NL}}$. The resulting values are then averaged.

To validate the proposed method, the nonlinear SNR is also measured experimentally. In particular, the overall SNR is retrieved from the real-time DSP of the commercial transceiver, for each power level. The OSNR and the $\mathrm{SNR}_{\mathrm{TRX}}$ are instead measured from the power spectral densities measured by the OSA and a set of back-to-back data acquisitions, respectively. Particularly, the procedure to estimate $\mathrm{SNR}_{\mathrm{TRX}}$ is the one described in [51], yielding $\mathrm{SNR}_{\mathrm{TRX}} = 19.77\,\mathrm{dB}$. Hence, $\mathrm{SNR}_{\mathrm{NL}}$ is easily obtained from (1). The results are reported in Fig. 6(b), where the generalized SNR (GSNR) [52] is $\mathrm{GSNR} = (\mathrm{SNR}^{-1} - \mathrm{SNR}_{\mathrm{TRX}}{}^{-1})^{-1}$. Please note that the OSNR tends to saturate around the value of $26\,\mathrm{dB}$ at high power levels, due to the internal noise added by the transceiver, the BST and pre-amplifier EDFAs.

The measured values of $\mathrm{SNR}_{\mathrm{NL}}$ are finally compared to those estimated by (12), as shown in Fig. 6(c). The corresponding absolute estimation error is also reported. In general, the results obtained with the proposed method are consistent with the measured values. The absolute estimation error is always below $0.6\,\mathrm{dB}$ and characterized by a root-mean-square error (RMSE) of approximately $\sim 0.4\,\mathrm{dB}$. Moreover, the simple correction factor derived in (14) proves to be effective in mitigating the estimation bias induced by XCI in the considered transmission system.

B. Transmission over a 1100-km Link

The setup used for this experiment is very similar to that shown in Fig. 6(a), with minor adjustments to the system configuration. We transmit a DP-16QAM 64-Gbaud WDM signal consisting of $N_{\mathrm{ch}} = 30$ channels spaced by $\Delta f = 100\,\mathrm{GHz}$. The per-channel power P_{ch} is varied between $-1\,\mathrm{dBm}$ and $5\,\mathrm{dBm}$ with step $2\,\mathrm{dB}$. In this experiment, the proposed method is applied to three COIs, centered at $191.8\,\mathrm{THz}$, $193.2\,\mathrm{THz}$ and $194.7\,\mathrm{THz}$, corresponding to one of the center channels and those at the two extremes of the WDM comb. This serves as an experimental validation of (15), as these channels typically experience the most varied XCI contributions to NLI during propagation. The signal is then propagated over an optical link of $N = 17$ SSMF spans, each

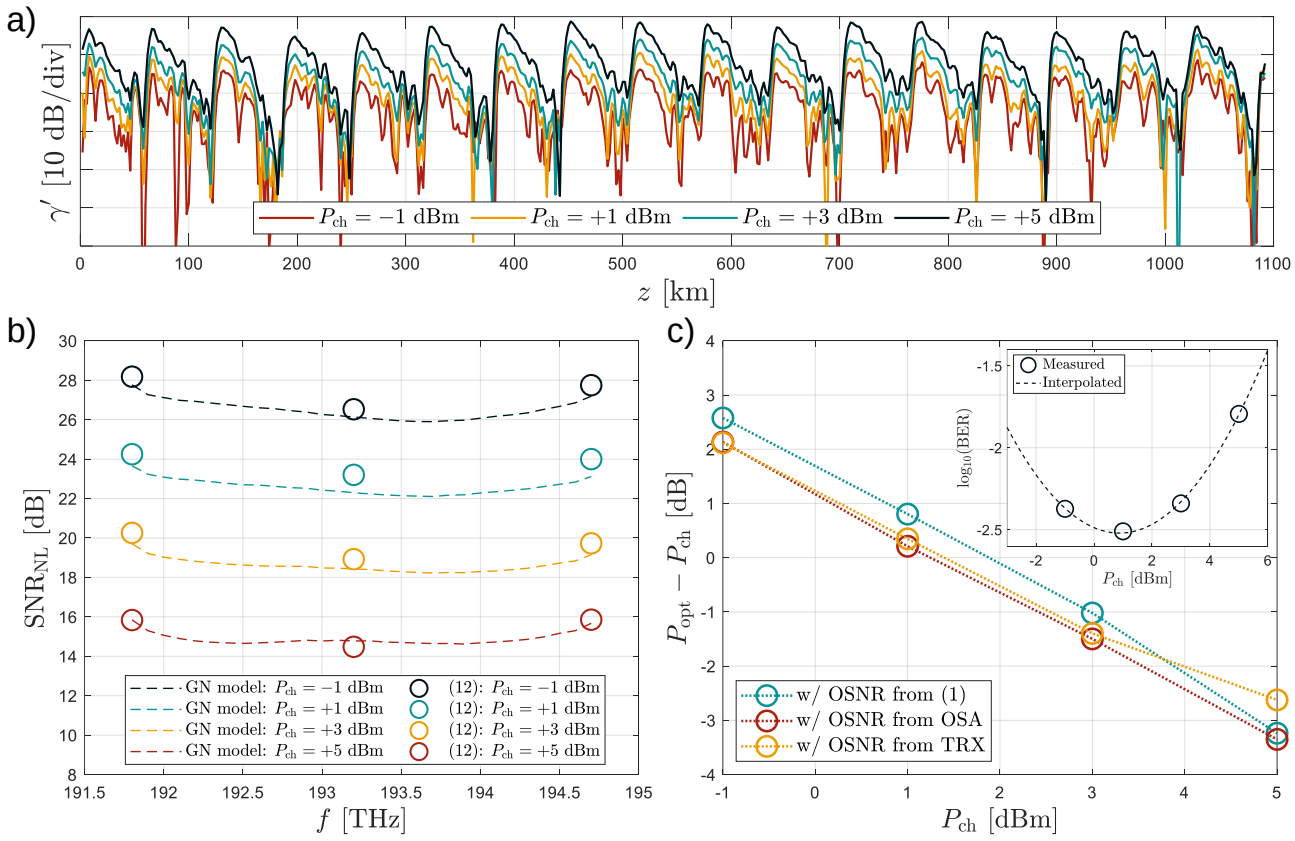

Fig. 7: a) Average relative power profiles γ' for all tested per-channel power levels. b) Comparison between estimated SNR$_{\mathrm{NL}}$ (circles) and the CFM GN-model (dashed line) after propagation over the 17×65-km link. c) Distance from optimal per–channel power P_{opt} – computed starting from estimated SNR$_{\mathrm{NL}}$ and considering the OSNR from (1), that provided by the commercial transceiver and that measured from OSA – based on the 3-dB rule. In the inset, the real optimal power based on the BER supplied by the commercial transceiver is reported.

with nominal length of $L_s = 65\,\mathrm{km}$. It is then processed as in Section IV-A, with the only difference that the CPR stage is implemented according to a BPS strategy. The number of samples at the input of the LPM algorithm is approximately 2^{17}, with a spatial step of $\Delta z = 2\,\mathrm{km}$. For each tested channel and power level, 100 profiles have been estimated and used in the computation of SNR$_{\mathrm{NL}}$. The averaged power profiles for the first WDM channel are displayed in Fig.7(a). The final SNR$_{\mathrm{NL}}$ estimate is given by the average of the resulting values.

We used two approaches to validate the proposed method in this scenario. The first involves a direct comparison of the estimated values with those obtained from the CFM model [5]. Note that this implementation, unlike the one used in Section II-C and Section III-B, includes the contribution of the modulation format. For this purpose, all the main fiber parameters required by the NLI model, such as α, β_2 and γ, were measured for each of the 17 spans in the optical link; while α and β_2 were measured with the aid of an OTDR, γ was measured with the method described in [51]. This approach was chosen due to the higher measurement uncertainties in the experimental setup, which made it difficult to reliably measure the values of SNR$_{\mathrm{NL}}$, as done in Section IV-A. Therefore, we opted to use a well-established NLI model, instead. The first set of results, shown in Fig. 7(b), indicates a mean absolute error of approximately $\sim 0.5\,\mathrm{dB}$ across all estimations, with an RMSE value around $0.6\,\mathrm{dB}$. In all cases, the maximum error remains below $0.9\,\mathrm{dB}$. Notably, the correction proposed in (15) effectively captures the different NLI evolution of the COIs also in this challenging scenario.

The second validation approach adopts a more practical perspective, which consists in assessing the accuracy of launch power optimization based on noise segregation, utilizing the SNR$_{\mathrm{NL}}$ values estimated with the proposed method. A comprehensive noise segregation is performed on the first channel of the WDM comb, utilizing the constellation SNR provided by the transceiver, the SNR$_{\mathrm{TRX}}$ estimated through the procedure outlined in Sec. IV-A (measured as SNR$_{\mathrm{TRX}} = 19.59\,\mathrm{dB}$ in this experiment), the nonlinear SNR$_{\mathrm{NL}}$ derived from (12), and the corresponding OSNR calculated by properly inverting (1). It is important to note that the OSNR obtained from (1) represents an indirect measure, meaning that its accuracy is influenced by errors in the other estimated parameters.

To specifically validate the estimated SNR$_{\mathrm{NL}}$, the same procedure is also repeated using OSNR values obtained from both an optical spectrum analyzer (OSA) and the commercial transceiver. In fact, the specific commercial transceiver employed in the experiment is capable of providing a direct esti-

mate of the OSNR after transmission [18]. This enables launch power optimization based on direct OSNR measurements, which are typically more accurate than indirect ones. The proposed methodology allows for a more robust validation of the estimated $\mathrm{SNR_{NL}}$ values and their practical applicability, showing how the result of the power optimization is affected by different accuracy levels in the terms involved.

Leveraging these measures and the so-called "3-dB rule"[1] [53]–[55], it is possible to get an estimate of how far, in terms of optical transmit power, the current working point is from the optimum, here denoted as P_{opt}. The expression for $P_{\mathrm{opt}} - P_{\mathrm{ch}}$, in dB units, can be written as:

$$P_{\mathrm{opt}} - P_{\mathrm{ch}} = \frac{1}{3}\left(\mathrm{SNR_{NL}} - \mathrm{OSNR} - 3\right). \tag{16}$$

This expression offers two important advantages. First, it is straightforward to evaluate in this scenario since all the required quantities are provided by the transceiver and the NLI estimation method. Moreover, the factor $1/3$ acts as a mitigation factor for errors in the estimation of OSNR and $\mathrm{SNR_{NL}}$ [10, Sec. IV-A]. This is clearly illustrated in Fig. 7(c), where (16) is evaluated using the OSNR from (1), the commercial transceiver and the OSA. An inset displaying the BER curve retrieved from the transceiver is also included. Here, BER serves as a performance metric to identify the optimal working point, located around $P_{\mathrm{opt}} \simeq +1\,\mathrm{dBm}$. At this point, (16) estimates a distance of $\sim 0\,\mathrm{dB}$ from P_{opt}, confirming the reliability of the $\mathrm{SNR_{NL}}$ values estimated by the proposed method. It is to be noted that the accuracy of (16) slightly degrades when the OSNR is computed from (1), in agreement with the previous considerations on indirect measurements. This suggests that direct estimates of the two quantities are preferable to accurately perform noise segregation. In any case, this analysis is of practical use, since it gives an example of how these results can be applied to optimize the transmission parameters.

V. Conclusions

In this work, we introduced a novel method to estimate the power of Kerr-induced NLI in live coherent optical transmissions. This method leverages only the data already available at the receiver's DSP and is intrinsically linked to the LLS-based LPM algorithm. Not only does it deliver precise NLI estimates but also tracks the power evolution of the WDM channel, offering valuable information for network optimization at higher layers.

This method was tested through extensive numerical simulations and two distinct experimental scenarios involving 300-km and 1100-km transmissions. In all cases, the proposed approach provided accurate NLI estimates across various power levels, including the optimal ones and those typically challenging for LPM. The accuracy of the method was benchmarked against predictions of analytical NLI models and direct experimental measurements, demonstrating its effectiveness in the tested scenarios. Moreover, it was successfully tested in the prediction of the optimal launch power, a crucial parameter for network optimization.

However, the method has two primary limitations. First, it only estimates the portion of NLI originating from SCI. To estimate the total NLI, we derived simple analytical expressions that require limited knowledge of the system parameters. Second, a large amount of data is required, especially at low launch power levels. Nonetheless, we anticipate that, in a live network, both NLI power and launch power remain relatively stable. Therefore, the algorithm can be executed offline by periodically extracting data from the real-time receiver DSP.

Future work should focus on a more comprehensive analysis of the accuracy of this method across various scenarios and explore its potential for network optimization, particularly in ultra-wide band (UWB) contexts, where optimizing optical launch power remains an active area of research [55]–[57].

[1]Formally, the 3-dB rule is optimal only when applied to a single span, or to the end-to-end system in the case of all identical, equally-spaced channels, and identical spans [53], [54]. However, it proved to work relatively well and be quasi-optimal also under more general conditions, including standard C-band transmissions and more recently UWB transmissions (e.g., C+L+S+E systems) [55]. Given its simplicity, it will be the launch power optimization strategy employed in this work.

Acknowledgments

The authors would like to thank Antonio Mecozzi and Pierluigi Poggiolini for the useful discussions on NLI modeling, and Stefano Straullu for his help in the realization of the experiment. Portions of this work were presented at the ECOC 2024 conference [35].

References

[1] M. Jinno, "Elastic optical networking: Roles and benefits in beyond 100-gb/s era," *Journal of Lightwave Technology*, vol. 35, no. 5, pp. 1116–1124, 2017.

[2] D. Wang, Y. Song, Y. Zhang, X. Jiang, J. Dong, F. N. Khan, T. Sasai, S. Huang, A. P. T. Lau, M. Tornatore, and M. Zhang, "Digital twin of optical networks: A review of recent advances and future trends," *Journal of Lightwave Technology*, vol. 42, no. 12, pp. 4233–4259, 2024.

[3] M. S. Faruk and S. J. Savory, "Measurement informed models and digital twins for optical fiber communication systems," *Journal of Lightwave Technology*, vol. 42, no. 3, pp. 1016–1030, 2024.

[4] V. Curri, "GNPy model of the physical layer for open and disaggregated optical networking [invited]," *J. Opt. Commun. Netw.*, vol. 14, no. 6, pp. C92–C104, 06 2022.

[5] P. Poggiolini and M. Ranjbar-Zefreh, "Closed form expressions of the nonlinear interference for UWB systems," in *2022 European Conference on Optical Communication (ECOC)*, 2022, pp. 1–4.

[6] H. Buglia, M. Jarmolovičius, L. Galdino, R. I. Killey, and P. Bayvel, "A closed-form expression for the Gaussian noise model in the presence of Raman amplification," *Journal of Lightwave Technology*, vol. 42, no. 2, pp. 636–648, 2024.

[7] F. N. Hauske, M. Kuschnerov, B. Spinnler, and B. Lankl, "Optical performance monitoring in digital coherent receivers," *Journal of Lightwave Technology*, vol. 27, no. 16, pp. 3623–3631, 2009.

[8] S. J. Savory, "Digital coherent optical receivers: Algorithms and subsystems," *IEEE Journal of Selected Topics in Quantum Electronics*, vol. 16, no. 5, pp. 1164–1179, 2010.

[9] L. Minelli, G. Bosco, S. Straullu, A. Nespola, S. Piciaccia, and D. Pilori, "DSP-based inter-channel interference monitoring in flexible wavelength-routed networks," *J. Opt. Commun. Netw.*, vol. 16, no. 6, pp. 695–705, Jun 2024.

[10] P. Poggiolini, G. Bosco, A. Carena, V. Curri, Y. Jiang, and F. Forghieri, "The GN-model of fiber non-linear propagation and its applications," *Journal of Lightwave Technology*, vol. 32, no. 4, pp. 694–721, 2014.

[11] A. Alvarado, T. Fehenberger, B. Chen, and F. M. J. Willems, "Achievable information rates for fiber optics: Applications and computations," *Journal of Lightwave Technology*, vol. 36, no. 2, pp. 424–439, 2018.

[12] R. Dar, M. Feder, A. Mecozzi, and M. Shtaif, "Pulse collision picture of inter-channel nonlinear interference in fiber-optic communications," *Journal of Lightwave Technology*, vol. 34, no. 2, pp. 593–607, 2016.

[13] D. Lippiatt, S. Varughese, T. Richter, S. Tibuleac, and S. E. Ralph, "Joint linear and nonlinear noise estimation of optical links by exploiting carrier phase recovery," in *2020 Optical Fiber Communications Conference and Exhibition (OFC)*, 2020, pp. 1–3.

[14] F. J. Caballero, D. J. Ives, C. Laperle, D. Charlton, Q. Zhuge, M. O'Sullivan, and S. J. Savory, "Machine learning based linear and nonlinear noise estimation," *Journal of Optical Communications and Networking*, vol. 10, no. 10, pp. D42–D51, 2018.

[15] A. D. Shiner, M. E. Mousa-Pasandi, M. Qiu, M. A. Reimer, E. Y. Park, M. Hubbard, Q. Zhuge, F. J. V. Caballero, and M. O'Sullivan, "Neural network training for OSNR estimation from prototype to product," in *Optical Fiber Communication Conference (OFC) 2020*. Optica Publishing Group, 2020, p. M4E.2.

[16] G. D. Rosa, S. Dris, and A. Richter, "Statistical quantification of nonlinear interference noise components in coherent systems," *Opt. Express*, vol. 28, no. 4, pp. 5436–5447, Feb 2020.

[17] Z. Dong, A. P. T. Lau, and C. Lu, "OSNR monitoring for QPSK and 16-QAM systems in presence of fiber nonlinearities for digital coherent receivers," *Opt. Express*, vol. 20, no. 17, pp. 19 520–19 534, Aug 2012.

[18] C. Rasmussen and M. Aydinlik, "Optical signal-to-noise ratio (OSNR) monitoring and measurement in optical communications sytems," Dec. 19 2017, US Patent 9,847,833.

[19] F. J. Vaquero-Caballero, D. J. Ives, and S. J. Savory, "Perturbation-based frequency domain linear and nonlinear noise estimation," *Journal of Lightwave Technology*, vol. 40, no. 18, pp. 6055–6063, 2022.

[20] J. Lu, G. Zhou, J. Zhou, and C. Lu, "Joint linear and nonlinear noise monitoring techniques based on spectrum analysis," *Opt. Express*, vol. 28, no. 24, pp. 36 953–36 971, Nov 2020.

[21] H. J. Cho, D. Lippiatt, V. A. Thomas, S. Varughese, S. Searcy, T. Richter, S. Tibuleac, and S. E. Ralph, "Constellation-based identification of linear and nonlinear OSNR using machine learning: a study of link-agnostic performance," *Opt. Express*, vol. 30, no. 2, pp. 2693–2710, 01 2022.

[22] M. Al-Nahhal, I. Al-Nahhal, O. A. Dobre, and S. K. O. Soman, "Parallel neural network structures for signal-to-noise ratio estimation in optical fiber communication systems," *Journal of Lightwave Technology*, vol. 42, no. 6, pp. 1941–1954, 2024.

[23] M. Boertjes, A. S. Kashi, J. C. Cartledge, and W.-Y. Chan, "Machine learning model training framework for nonlinear signal-to-noise ratio estimation in heterogeneous optical networks," *Journal of Lightwave Technology*, pp. 1–11, 2024.

[24] I. Andrenacci, M. Lonardi, P. Ramantanis, Élie Awwad, E. Irurozki, S. Clémençon, and S. Almonacil, "Machine-learning-based technique to establish ASE or Kerr impairment dominance in optical transmission," *J. Opt. Commun. Netw.*, vol. 16, no. 4, pp. 481–492, Apr 2024.

[25] R. Dar and P. J. Winzer, "Nonlinear interference mitigation: Methods and potential gain," *Journal of Lightwave Technology*, vol. 35, no. 4, pp. 903–930, 2017.

[26] M. S. Neves, A. Lorences-Riesgo, C. S. Martins, S. Mumtaz, G. Charlet, P. P. Monteiro, and F. P. Guiomar, "Carrier-phase recovery for coherent optical systems: Algorithms, challenges and solutions," *Journal of Lightwave Technology*, vol. 42, no. 3, pp. 1095–1108, 2024.

[27] T. Tanimura, S. Yoshida, K. Tajima, S. Oda, and T. Hoshida, "Fiber-longitudinal anomaly position identification over multi-span transmission link out of receiver-end signals," *Journal of Lightwave Technology*, vol. 38, no. 9, pp. 2726–2733, 2020.

[28] T. Sasai, M. Takahashi, M. Nakamura, E. Yamazaki, and Y. Kisaka, "Linear least squares estimation of fiber-longitudinal optical power profile," *Journal of Lightwave Technology*, vol. 42, no. 6, pp. 1955–1965, 2024.

[29] T. Sasai, M. Takahashi, R. Kaneko, Y. Sone, M. Nakamura, and E. Yamazaki, "Recent advances in digital longitudinal monitoring of fiber-optic link," in *2024 Optical Fiber Communications Conference and Exhibition (OFC)*, 2024, pp. 1–3.

[30] T. Sasai, M. Nakamura, E. Yamazaki, S. Yamamoto, H. Nishizawa, and Y. Kisaka, "Digital longitudinal monitoring of optical fiber communication link," *Journal of Lightwave Technology*, vol. 40, no. 8, pp. 2390–2408, 2022.

[31] L. Andrenacci, G. Bosco, and D. Pilori, "PDL localization and estimation through linear least squares-based longitudinal power monitoring," *IEEE Photonics Technology Letters*, vol. 35, no. 24, pp. 1431–1434, 2023.

[32] J. Chang, C. Hahn, X. Tang, T. Zhao, W. C. Ng, and Z. Jiang, "Demonstration of longitudinal power profile estimation using commercial transceivers and its practical consideration," in *49th European Conference on Optical Communications (ECOC 2023)*, 2023, pp. 1334–1337.

[33] I. Kim, K. Sone, O. Vassilieva, S. Oda, P. Palacharla, and T. Hoshida, "Nonlinear SNR estimation based on power profile estimation in hybrid Raman-EDFA link," in *Optical Fiber Communication Conference (OFC) 2024*. Optica Publishing Group, 2024, p. Th1F.6.

[34] V. Curri, A. Carena, A. Arduino, G. Bosco, P. Poggiolini, A. Nespola, and F. Forghieri, "Design strategies and merit of system parameters for uniform uncompensated links supporting Nyquist-WDM transmission," *Journal of Lightwave Technology*, vol. 33, no. 18, pp. 3921–3932, 2015.

[35] L. Andrenacci, G. Bosco, Y. Jiang, A. Nespola, S. Straullu, S. Piciaccia, and D. Pilori, "Nonlinear noise estimation using linear least squares-based longitudinal power monitoring," in *50th European Conference on Optical Communications (ECOC 2024)*, 2024, p. M3E.4.

[36] A. Vannucci, P. Serena, and A. Bononi, "The RP method: a new tool for the iterative solution of the nonlinear schrodinger equation," *Journal of Lightwave Technology*, vol. 20, no. 7, pp. 1102–1112, 2002.

[37] P. Serena and A. Bononi, "An alternative approach to the Gaussian noise model and its system implications," *Journal of Lightwave Technology*, vol. 31, no. 22, pp. 3489–3499, 2013.

[38] Y. Jiang, D. Tang, Z. Wang, J. Luo, B. Zheng, and Y. Qiao, "Symbol-level fiber-longitudinal power profile estimation," *Opt. Lett.*, vol. 49, no. 9, pp. 2305–2308, May 2024. [Online]. Available: https://opg.optica.org/ol/abstract.cfm?URI=ol-49-9-2305

[39] C. Malouin, P. Thomas, B. Zhang, J. O'Neil, and T. Schmidt, "Natural expression of the best-match search godard clock-tone algorithm for blind chromatic dispersion estimation in digital coherent receivers," in *Advanced Photonics Congress*. Optica Publishing Group, 2012, p. SpTh2B.4.

[40] D. Pilori, M. Cantono, A. Carena, and V. Curri, "FFSS: The fast fiber simulator software," in *2017 19th International Conference on Transparent Optical Networks (ICTON)*, Girona, Spain, 2017, pp. 1–4.

[41] P. Poggiolini, "The GN model of non-linear propagation in uncompensated coherent optical systems," *Journal of Lightwave Technology*, vol. 30, no. 24, pp. 3857–3879, 2012.

[42] L. Andrenacci, G. Bosco, and D. Pilori, "Longitudinal power monitoring performance with subcarrier multiplexing transmission," in *2023 IEEE Photonics Conference (IPC)*, 2023, pp. 1–2.

[43] I. Kim, O. Vassilieva, R. Shinzaki, M. Eto, S. Oda, and P. Palacharla, "Multi-channel longitudinal power profile estimation," in *49th European Conference on Optical Communications (ECOC 2023)*, vol. 2023, 2023, pp. 491–494.

[44] R. Dar, M. Feder, A. Mecozzi, and M. Shtaif, "Properties of nonlinear noise in long, dispersion-uncompensated fiber links," *Opt. Express*, vol. 21, no. 22, pp. 25 685–25 699, Nov 2013.

[45] ——, "Accumulation of nonlinear interference noise in fiber-optic systems," *Opt. Express*, vol. 22, no. 12, pp. 14 199–14 211, Jun 2014.

[46] A. Carena, G. Bosco, V. Curri, Y. Jiang, P. Poggiolini, and F. Forghieri, "EGN model of non-linear fiber propagation," *Opt. Express*, vol. 22, no. 13, pp. 16 335–16 362, Jun 2014.

[47] R. Eisenach. "ASE noise loading for terrestrial WDM applications". Nokia. Accessed: Dec 4, 2024. [Online]. Available: https://www.nokia.com/blog/ase-noise-loading-for-terrestrial-wdm-applications/

[48] P. Poggiolini, A. Nespola, Y. Jiang, G. Bosco, A. Carena, L. Bertignono, S. M. Bilal, S. Abrate, and F. Forghieri, "Analytical and experimental results on system maximum reach increase through symbol rate optimization," *Journal of Lightwave Technology*, vol. 34, no. 8, pp. 1872–1885, 2016.

[49] Ciena. "WaveLogic 6". Accessed: Dec 4, 2024. [Online]. Available: https://www.ciena.com/products/wavelogic/wavelogic-6

[50] T. Richter, J. Pan, and S. Tibuleac, "Comparison of WDM bandwidth loading using individual transponders, shaped, and flat ASE noise," in *Optical Fiber Communication Conference*. Optica Publishing Group, 2018, p. W1B.2.

[51] Y. Jiang, A. Nespola, S. Straullu, F. Forghieri, S. Piciaccia, A. Tanzi, M. R. Zefreh, G. Bosco, and P. Poggiolini, "Experimental test of a closed-form EGN model over C+L bands," *Journal of Lightwave Technology*, pp. 1–11, 2024.

[52] A. Pilipetskii, D. Kovsh, E. Mateo, E. R. Hartling, G. Mohs, L. Jovanovski, M. Salsi, M. Cantono, M. Bolshtyansky, O. Courtois, O. Gautheron, O. A. Sab, P. Pecci, P. Mehta, S. Grubb, T. Inoue, V. Kamalov, V. Vusirikala, V. Letellier, and Y. Inada, "The subsea fiber as a shannon channel," in *SubOptic 2019*, 2019.

[53] G. Bosco, A. Carena, R. Cigliutti, V. Curri, P. Poggiolini, and F. Forghieri, "Performance prediction for WDM PM-QPSK transmission over uncompensated links," in *Optical Fiber Communication Con-*

ference/National Fiber Optic Engineers Conference 2011. Optica Publishing Group, 2011, p. OThO7.

[54] E. Grellier and A. Bononi, "Quality parameter for coherent transmissions with Gaussian-distributed nonlinear noise," *Opt. Express*, vol. 19, no. 13, pp. 12 781–12 788, Jun 2011.

[55] Y. Jiang, F. Forghieri, S. Piciaccia, G. Bosco, and P. Poggiolini, "Optimum launch power in multiband systems," in *50th European Conference on Optical Communications (ECOC 2024)*, 2024, p. W2A.84. [Online]. Available: https://arxiv.org/abs/2407.08309

[56] H. Buglia, E. Sillekens, A. Vasylchenkova, P. Bayvel, and L. Galdino, "On the impact of launch power optimization and transceiver noise on the performance of ultra-wideband transmission systems [invited]," *J. Opt. Commun. Netw.*, vol. 14, no. 5, pp. B11–B21, May 2022.

[57] S. Escobar-Landero, A. Lorences-Riesgo, X. Zhao, Y. Frignac, and G. Charlet, "S+C+L high-capacity transmission systems: Challenges and opportunities," *Journal of Lightwave Technology*, vol. 42, no. 12, pp. 4260–4270, 2024.